NASA/TM—2017-219440

Increased Jet Noise Due to a "Nominally Laminar" State of Nozzle Exit Boundary Layer

K.B.M.Q. Zaman
Glenn Research Center, Cleveland, Ohio

January 2017

NASA STI Program . . . in Profile

Since its founding, NASA has been dedicated to the advancement of aeronautics and space science. The NASA Scientific and Technical Information (STI) Program plays a key part in helping NASA maintain this important role.

The NASA STI Program operates under the auspices of the Agency Chief Information Officer. It collects, organizes, provides for archiving, and disseminates NASA's STI. The NASA STI Program provides access to the NASA Technical Report Server—Registered (NTRS Reg) and NASA Technical Report Server—Public (NTRS) thus providing one of the largest collections of aeronautical and space science STI in the world. Results are published in both non-NASA channels and by NASA in the NASA STI Report Series, which includes the following report types:

- TECHNICAL PUBLICATION. Reports of completed research or a major significant phase of research that present the results of NASA programs and include extensive data or theoretical analysis. Includes compilations of significant scientific and technical data and information deemed to be of continuing reference value. NASA counter-part of peer-reviewed formal professional papers, but has less stringent limitations on manuscript length and extent of graphic presentations.

- TECHNICAL MEMORANDUM. Scientific and technical findings that are preliminary or of specialized interest, e.g., "quick-release" reports, working papers, and bibliographies that contain minimal annotation. Does not contain extensive analysis.

- CONTRACTOR REPORT. Scientific and technical findings by NASA-sponsored contractors and grantees.

- CONFERENCE PUBLICATION. Collected papers from scientific and technical conferences, symposia, seminars, or other meetings sponsored or co-sponsored by NASA.

- SPECIAL PUBLICATION. Scientific, technical, or historical information from NASA programs, projects, and missions, often concerned with subjects having substantial public interest.

- TECHNICAL TRANSLATION. English-language translations of foreign scientific and technical material pertinent to NASA's mission.

For more information about the NASA STI program, see the following:

- Access the NASA STI program home page at http://www.sti.nasa.gov

- E-mail your question to help@sti.nasa.gov

- Fax your question to the NASA STI Information Desk at 757-864-6500

- Telephone the NASA STI Information Desk at 757-864-9658

- Write to:
  NASA STI Program
  Mail Stop 148
  NASA Langley Research Center
  Hampton, VA 23681-2199

NASA/TM—2017-219440

Increased Jet Noise Due to a "Nominally Laminar" State of Nozzle Exit Boundary Layer

K.B.M.Q. Zaman
Glenn Research Center, Cleveland, Ohio

National Aeronautics and
Space Administration

Glenn Research Center
Cleveland, Ohio 44135

January 2017

Acknowledgments

Help from Dr. Cliff Brown in data acquisition in the AAPL is gratefully acknowledged. Thanks are due to Dr. James Bridges for helpful inputs during the course of the study, and to Dr. Amy Fagan for help with the schlieren data acquisition. The work was supported by the Commercial Supersonics Technology (CST) Project under NASA's Advanced Air Vehicles Program.

Level of Review: This material has been technically reviewed by technical management.

Available from

NASA STI Program
Mail Stop 148
NASA Langley Research Center
Hampton, VA 23681-2199

National Technical Information Service
5285 Port Royal Road
Springfield, VA 22161
703-605-6000

This report is available in electronic form at http://www.sti.nasa.gov/ and http://ntrs.nasa.gov/

Increased Jet Noise Due to a "Nominally Laminar" State of Nozzle Exit Boundary Layer

K.B.M.Q. Zaman
National Aeronautics and Space Administration
Glenn Research Center
Cleveland, Ohio 44135

Abstract

A set of 2-in. diameter nozzles is used to investigate the effect of varying exit boundary layer state on the radiated noise from high-subsonic jets. It is confirmed that nozzles involving turbulent boundary layers are the quietest while nozzles involving a "nominally laminar" boundary layer are loud especially on the high-frequency side of the sound pressure level spectrum. The latter boundary layer state involves a "Blasius-like" mean velocity profile but higher turbulence intensities compared to those in the turbulent state. The higher turbulence in the initial region of the jet shear layer leads to increased high-frequency noise. The results strongly suggest that an anomaly noted with subsonic jet noise databases in the literature is due to a similar effect of differences in the initial boundary layer state.

Introduction

An anomaly was noted by Viswanathan (Ref. 1) among subsonic jet noise databases in the literature. The normalized amplitudes of sound pressure level spectra were higher in certain sets of data relative to other sets at same operating conditions. Figure 1, reproduced from (Ref. 1), illustrates the difference between the data of Tanna (Ref. 2) and those taken in a Boeing facility (Low-Speed Aero acoustic Facility, Ref. 1). Data from Reference 2 exhibit consistently higher amplitudes on the high-frequency end. The contrast between data from "University-type" facilities (Refs. 2 to 5) and "Industrial-type" facilities (Refs. 1, 6, and 7) was further identified and discussed by Harper-Bourne (Ref. 8). It had been speculated in Reference 1 that perhaps higher upstream rig noise in the facility of Reference 2 caused the higher noise. However, Harper-Bourne convincingly ruled this out while noting that databases exhibiting higher noise were taken in facilities having large contraction ratios (Ref. 8). Why would contraction ratio affect noise, however, remained unanswered and the basic reason for the anomaly remained unexplained. The issue is important since these databases are foundations for validation of jet noise prediction codes.

Probable causes for the anomaly were explored in an earlier study (Ref. 9). Among other parameters, turbulence intensity in the jet core and internal geometry of the nozzle were varied and corresponding effects on noise were studied. Core turbulence was varied over a range of 0.15 to 0.5 percent by using turbulence generating grids upstream of the nozzle. Amplitudes of far-field noise spectra were found to increase with increasing core turbulence. This observation ruled out the latter parameter as the source of the anomaly noted above. The University-type facilities had large contraction ratios as well as flow conditioning units so that the turbulence at the jet exit was minimized, whereas those were the ones that yielded higher noise.

Taking a cue from an observation made in Reference 10, the effect of nozzle interior shape was examined in Reference 9. In Reference 10, with data taken in the same facility, a nozzle with "ASME" interior shape was noted to generate higher noise levels compared to that from a nozzle with a "conic" interior shape. Two small nozzles were fabricated mimicking those interior shapes and a similar difference in the noise levels was confirmed (Ref. 9). It was then shown that the ASME nozzle involved a nominally laminar initial boundary layer as opposed to a turbulent boundary layer with the conic nozzle. A nominally laminar boundary layer has a Blasius-like mean velocity profile, as with a laminar flat-plate boundary layer (Ref. 11), but involves high turbulence intensities—even higher than that in a turbulent

case. Apparently it is a transitional state involving high intermittency. Transitional states of boundary layers are expected at low Mach and Reynolds numbers that may affect noise and other jet properties (Ref. 12). What was rather unexpected was the fact that the nominally laminar state persisted throughout the Mach number range covered in Reference 9 (up to 1, corresponding to jet Reynolds numbers based on nozzle diameter of about 0.70×10^6). The turbulence intensity in the initial boundary layer as well as the radiated noise were consistently larger with the ASME case relative to the conic case throughout the range. While no boundary layer data were presented along with the cited databases (Refs. 1 to 7), it was conjectured in Reference 9 that a difference in the initial state might be at the root of the observed anomaly in the noise amplitudes.

However, questions lingered. The nozzles used in Reference 9 had 1 in. exit diameters (D = 1 in.). In the previous works (Refs. 1 to 7), mostly 2 in. diameter nozzles were used. The facility used in Reference 9 was semi-anechoic and data were examined only at limited microphone locations. An accurate set of noise spectra and directivity data were desirable to confirm the effect of the initial state. This led to a continuation of the experiment. A set of 2 in. diameter nozzles was fabricated with designs intended to vary the initial boundary layer state systematically. Boundary layer data as well as preliminary noise data were acquired in the same facility as used in Reference 9. Then for limited cases, high quality noise measurements were performed in an anechoic facility (NASA GRC Aeroacoustic Propulsion Laboratory, AAPL) in order to document accurate and detailed noise characteristics. These results are presented in this technical memorandum. The nozzle coordinates, boundary layer as well as sound pressure level spectral data are also provided in digital format in the accompanying CD/DVD-ROM (available online from www.sti.nasa.gov) for anyone interested in further analysis.

Experimental Procedure

All flow-field data and limited noise data are gathered in the "CW17" open jet facility at NASA GRC (Ref. 9). A picture is shown in Figure 2(a). Compressed air passes through a 30 in. diameter plenum and through the nozzle to discharge into the quiescent ambient of the test chamber. With the large contraction ratio and the flow conditioning units this facility falls into the University-type category as referred to in the Introduction.

All nozzles used in the study are convergent. Pictures of the conic and the "ASME design" nozzles are shown in Figures 2(b) and (c), respectively. The internal contours of these two nozzles are shown in Figure 3; (the rest of Fig. 2 is discussed shortly). While detailed contours of all nozzles are given in the digital files, the salient features of the nozzles are discussed here. The upstream section of all nozzles, which attaches to the plenum chamber, starts with a diameter of 5.16 in. The conic case contracts down to a 2.558 in. diameter cylindrical section (blue line in Fig. 3(a)), at the end of which is the conical section (light blue line). The conical section contracts down to 2 in. diameter exit over a length of 3.32 in.; thus, the half-angle of convergence is 4.8°.

The interior contour of each ASME case has a common 4.66 in. diameter cylindrical section of length 3.5 in. (green line in Fig. 3(b)). At its end, end-pieces of various designs could be attached. The combination of blue and red lines at the end of Figure 3(b) represents the end-piece for the ASME design nozzle. The convergence takes place over the length of the blue line while the red line at the end is a cylindrical section. The contours of all four ASME end-pieces, namely, ASME long, design, short and short-with-extension, are shown in Figure 3(c). With the long case, the convergence takes place over a long length terminating in a short cylindrical section. Both the short and short-with-extension cases have identical convergent section; the latter one has a longer cylindrical section. For identification in the figures, the four ASME cases will be abbreviated as "Long", "Dsgn", "Shrt" and "Sh-e", respectively. All nozzles have 0.050 in. lip thickness at the exit.

The four ASME internal shapes are designed in an attempt to obtain varying boundary layer states at the exit. The black dots on the contours in Figure 3(c) represent locations where an acceleration parameter, $K = \nu \frac{dU}{dx} / U^2 * 10^6$, reaches a value of 2 (assuming $M_j = 0.96$, exit velocity = 1000 ft/s). In all cases, K starts with a large value (high flow acceleration) and becomes smaller than 2 downstream of the black dot. Per Reference 13, the boundary layer may be expected to stay laminar (or laminarize if initially turbulent) if $K>2$, while a turbulent boundary layer would be sustained for $K<2$. For the conic nozzle, the value of K is less than 0.2 for the entire length of the convergent section (Fig. 3(a)); thus, a turbulent boundary layer may be expected with this nozzle. With the ASME cases, on the other hand, varying degrees of convergence together with varying lengths of the cylindrical section may be expected to yield different transitional states of the boundary layer. However, the acceleration criterion, as with various other criteria found in the literature, is only a rough guideline for laminar-turbulent transition of a nozzle boundary layer. The transition phenomenon is still an unresolved area in aerodynamics, and only measurements can provide exact characteristics of the exit boundary layer.

Boundary layer measurements are done using the hot-wire technique using a Thermo Systems Inc. (TSI, IFA100) anemometer. A TSI-1260-10A miniature probe is used and the setup is shown in Figure 2(d). The sensor diameter and active length are 0.001 and 0.01 in., respectively; the prong-to-prong distance of the sensor is about 0.040 in. The measurements are made about 0.030 in. downstream of the nozzle exit. The probe is inserted at an angle and only the sensor and the prongs enter the boundary layer. It will be seen later that the ASME design case yields a nominally laminar boundary layer. Additional data are acquired with the latter nozzle together with a boundary layer trip. The tripping is done by a sleeve (Fig. 2(e)) that starts at an axial location of 4.96 in. (3.04 in. upstream from exit where the diameter is 1.81 in.) and stops at 5.739 in. (2.261 in. upstream from exit where the diameter is 1.20 in.). The sleeve is fabricated by 3-D printing and its thicknesses at the start and end are about 0.08 and 0.02 in., respectively. Transition is likely achieved by the 0.02 in. backward-facing step at $x = 5.739$ in. which is just past the location where $K = 2$ ($x = 5.70$ in.). As it will be seen, this yields a fully turbulent exit boundary layer. A few other trip sleeves ending at farther upstream locations were also found effective. However, the K criterion may be used only as a crude guideline for locating a trip; obviously the thickness of the boundary layer and its upstream history must come into play. The practice of nozzle boundary layer tripping largely remains an art. (Trips may not only be ineffective but sometimes produce undesirable tones. One trip sleeve in this experiment produced such a tone; it was simply avoided and not pursued further.)

Limited noise measurements are done in the CW17 facility (Fig. 2(a)). These data are taken with 1/4-in. (B&K) microphones placed at various polar locations θ (referenced to the jet's downstream axis). This facility is semi-anechoic and not suitable for high-quality noise measurements. However, for assessing relative changes in noise spectra with parametric variation the data quality is considered adequate. Noise data from this facility are shown mostly for θ = 90°, the microphone being located at 54.8 in. from the nozzle exit. A personal computer based data acquisition system with LabVIEW (National Instruments) software is used for the measurements. Detailed noise data are then acquired with a few of the nozzles in the Aeroacoustics Propulsion Laboratory (AAPL), a premier noise measurement facility at NASA. Description of this facility can be found in prior publications, e.g., (Ref. 7), and it is not repeated here. All data presented in the following pertain to subsonic, unheated flow; i.e., with total temperature the same throughout as in the ambient of the test chamber. The jet Mach number, $M_j = \left(\left((p_0 / p_a)^{(\gamma-1)/\gamma} - 1 \right) \frac{2}{\gamma - 1} \right)^{1/2}$, is used in the following as the independent variable; here, p_0 and p_a are plenum pressure and ambient pressure, respectively.

Results

Boundary Layer Data

Recall that a single hot-wire probe is used for obtaining the boundary layer data. Apart from sensor survivability, stability of the anemometer circuitry and occasional electronic noise due to strain-gaging effects, there are issues in the measurements in high-speed compressible flows. In such flows the hot-wire responds to the product of density and velocity rather than just velocity as in incompressible flows. With constant temperature anemometer operation, the sensitivity to temperature is thought to be small although at high M_j static temperature is significantly low and the extent of the temperature effect on the measurements remains unclear. The probe is calibrated at the nozzle exit against the jet velocity U_j calculated from the plenum pressure. In the measurements, a probe voltage is converted to velocity and then nondimensionalized by the jet velocity U_j. Since the probe actually responds to ρu, approximately $\rho U/\rho_j U_j$ is measured for the "mean velocity" and $(\rho u)'/\rho_j U_j$ is measured for the "turbulence intensity". The ratio $\rho U/\rho_j U_j$ is substituted for U/U_j in the integration to obtained boundary layer thicknesses. In view of the measurement difficulties and ambiguities, the profiles and thickness estimates should be considered as qualitative especially at high values of M_j. They are, however, considered adequate to capture the overall characteristics of the boundary layer and differentiate between laminar and turbulent states.

The velocity profiles for various nozzles are shown in Figures 4 to 9 for three jet Mach numbers (M_j) each. The mean velocity is shown by the (red) circular symbols and the turbulence intensity by the (blue) triangular symbols. The mean velocity scale is shown on the left while that for turbulence intensity is shown on the right; these scales pertain to all three M_j in each figure. The values of M_j, momentum thickness (δ_2) and peak turbulence intensity are shown in the legend of each figure. Since the data are taken somewhat downstream of the nozzle exit (~0.030 in.), the profiles do not end in zeroes on the low-speed side and have a "tail". In the integration for calculation of boundary layer thicknesses, the profiles are extrapolated from 60 and 40 percent velocity points to find the wall location; on the other end, the integration is truncated at 98 percent velocity point. Note that the data are shown only up to $M_j = 0.825$ in Figures 4 to 9. Another serious issue encountered with the hot-wire measurements at even higher M_j is discussed in the following.

For the conic nozzle case in Figure 4, the mean velocity is characteristic of a turbulent boundary layer at all M_j. The velocity decays gradually over a long distance until a sharp drop occurs near the wall. The shape factor (H_{12} = displacement thickness/momentum thickness), as further discussed later, turns out to be about 1.65 in all three cases. Note that the turbulence intensity is relatively low, with a peak value of about 6 percent that drops with increasing M_j. This value is much lower than corresponding value in a zero-pressure-gradient, incompressible, flat-plate boundary layer and appears to be typical of compressible nozzle flows. The spectral content of the velocity fluctuations are broadband (discussed in Reference 9 for geometrically similar but smaller nozzles; sample velocity traces are shown later). From these considerations the boundary layer for the conic nozzle is inferred to be turbulent.

Corresponding data for the ASME design case are shown in Figure 5. Here, the mean velocity profile is flat within the core of the jet and the boundary layer is thinner. However, the turbulence intensities are much larger than those for the conic case (Fig. 4). In spite of the large turbulence, the mean velocity remains unity until close to the wall (about $y/D = 0.48$). The mean velocity profiles bear similarity to the Blasius-profile of a laminar boundary layer. However, here, the shape factor turns out to be close to 2.0, a value smaller than that of a Blasius profile (2.59). In view of the fact that the profiles are measured downstream of the nozzle exit (yielding a "tan-h" type profile typical of a free shear layer), the large turbulence and possible compressibility effects, deviations may not be unexpected. The truncation at 98 percent point, necessitated by some uncertainties in the data due to a temperature effect discussed shortly, also contributed somewhat to the lower value of H_{12} (displacement thickness is underestimated more than momentum thickness). In any case, the mean velocity profile is considered laminar-like while the turbulence intensity is high. This is the state that was referred to as nominally laminar or "highly

disturbed laminar" in References 9 and 13. An interested reader may look up the cited references for further discussions of nozzle boundary layer states, based mostly on data from incompressible flows.

The most conspicuous feature of the nominally laminar (or highly disturbed laminar) state is the high turbulence intensity – much higher than that found in a fully turbulent state. Peak values in some cases may exceed 15 percent. Sometimes the u'-profile is characterized by a "double peak" as seen in Figure 5. For the ASME design nozzle in the present experiment, this state persisted throughout the M_j range covered (up to $M_j = 1$, corresponding to $Re_D \approx 1.4\times10^6$).

Corresponding data for the ASME long case are shown in Figure 6. Essentially similar characteristics are noted as with the ASME design case and the boundary layer for this nozzle is also inferred to be nominally laminar. Corresponding data shown in Figure 7 for the ASME short case exhibit a somewhat surprising trend. Referring back to Figure 3, it can be seen that the length of the flow path downstream of the $K = 2$ point is the shortest for this nozzle. Hence a more laminar-like boundary layer was expected. The mean-velocity profiles in Figure 7 do exhibit a thin boundary layer with laminar-like behavior as with the design and the long cases. However, the turbulence intensity is nowhere near as large. On the other hand, for the short case with long extension (Sh-e) it is clear that the boundary layer is turbulent (Fig. 8). The mean velocity decay occurs over a long distance, the momentum thickness is much larger and the trends are comparable to those seen for the conic case in Figure 4. Finally, when the boundary layer of the ASME design case is tripped it also becomes turbulent as evident from Figure 9.

Data at higher M_j values (up to 1) were taken for all nozzles and for most cases the overall features of the profiles remained the same as discussed above. However, in all cases a near-wall "bump" appeared in the mean velocity profile. Examples of this at $M_j = 0.96$ are shown for three nozzles in Figure 10. The bump, more pronounced with the ASME design case, involved values of $U/U_j > 1$ over a small radial extent near the edge of the boundary layer. Presumably it occurred due to some thermal effect leading to hot-wire errors (the jet core at this M_j was about 84 °F colder than ambient); however, the exact reason remained unclear. Note that the pattern for the turbulence intensity has remained the same as seen at lower Mach numbers; for example, compare Figure 10(a) with Figure 5. Boundary layer tripping did not eliminate the bump (Fig. 10(b)). It appeared less pronounced with a thicker turbulent boundary layer (Fig. 10(c)). The bump had a large effect on the integral thickness estimates; the truncation criterion for the integration became ambiguous and the thickness turned out to be smaller. Thus, the results for $M_j > 0.825$ are not included in further discussions. However, one more set of data on the issue is shown in Figure 11 in order to illustrate that the bump is an artifact of hot-wire issues and not real.

The thick boundary layer with the Sh-e case allowed measurements with Pitot and static pressure probes with good spatial resolution. Velocity profile deduced from those data are compared with the hot-wire data in Figure 11(a). Corresponding total and static pressure profiles are shown in Figure 11(b). (The Pitot probe had a 0.01 in. flattened tip while a "Pinckney" probe with 0.043 in. outer diameter was used for the static pressure data; the two pressure profiles were obtained in separate runs). The bump is not seen with the velocity profile from the Pitot-static measurements (Fig. 11(a)). The characteristics of the bump changed somewhat with different overheat ratio or even when a different hot-wire was used. Thus, it was inferred to be due to some thermal effect. Because of sensor breakages the issue was abandoned and not pursued any further.

Characteristic boundary layer data as a function of M_j are shown in Figure 12 for the six cases covered in Figures 4 to 9. The nozzles are identified in the legend shown at the bottom in Figure 12(c). Momentum thickness versus M_j data are plotted in Figure 12(a). At large M_j, the values are small for the ASME design, long as well as the short cases. With turbulent boundary layer, it is thick for the conic, tripped and the ASME short-with-extension cases. It is the thickest for the last (Sh-e) case. On the low end of M_j, the values for the conic case are small. Apparently the boundary layer for the conic nozzle goes through transition around $M_j = 0.3$; a similar but sharper transition occurred at about the same M_j with the smaller conic nozzle in Reference 9.

Corresponding shape factor (H_{12}) data are plotted in Figure 12(b). For the conic case with turbulent boundary layer H_{12} is relatively small and has values in the range of 1.6 to 1.7. For the ASME design case it is in the range of 1.9 to 2.0. The values for the other cases fall between these two limits. Data for the Sh-e case is near the lower limit. For the ASME short case, the values are near the higher limit. Thus, just based on the H_{12} results it is difficult to make clear inferences on the boundary layer state. Perhaps, the parameter that best describes the boundary layer state, which also impacts the noise radiation, is the turbulence intensity. Peak turbulence intensity data are shown in Figure 12(c). Over most of the M_j-range covered, the peak intensity is large for the design and long cases, indicating a nominally laminar state. For the conic nozzle, the trend is consistent with transition taking place around $M_j = 0.3$; peak intensity drops with increasing M_j as the turbulent state is reached. With further increase in M_j there is a slight increase in thickness but a slight decrease in turbulence. For the Sh-e and the trip cases the intensity is also low throughout the M_j-range. For the short case, the intensity is low, the thickness small, while H_{12} is high. This may suggest a laminar state but velocity traces shown in the next figure indicate otherwise.

Sample velocity traces obtained at 94 percent velocity point in the boundary layer are shown in Figure 13, for the ASME design, conic and short cases, in (a), (b) and (c), respectively. For the design case in (a) the fluctuation amplitudes are large. Note that the skewness of the signal, denoted in the legend, is negative with a large amplitude ($s = –1.55$). Comparatively, the fluctuation amplitudes and the value of s are smaller with the conic case in Figure 13(b). Recall that the short case might have appeared laminar from the δ_2 and H_{12} data. It was thought that the intensity (Fig. 7(a)) might be due to low frequency unsteady fluctuations. However, the velocity trace in Figure 13(c) shows that it is turbulent with high frequency content just as seen with the conic case. Thus, an inspection of the velocity signal is also necessary in order to make inferences on the boundary layer state. The boundary layer for the short case is thin but inferred to be turbulent at $M_j = 0.31$.

Another aspect is worth noting again: the velocity traces are highly skewed with the nominally laminar case, leading to large deviations in the value of s. Large negative spikes mark the velocity traces on the high-speed edge of the boundary layer yielding large negative s, while large positive spikes mark the traces on the low-speed side (say, around 10 percent velocity point as shown in Reference 9, yielding large positive s). These are indicative of an unsteady transitional state with high intermittency. The spectra, however, do not exhibit any dominant peak (Ref. 9).

With regards to the nominally laminar state another question came up. Recalling that the measurements are done 0.030 in. downstream of the nozzle lip, the question was if the boundary layer inside the nozzle had the same characteristic as seen at the measurement station or if a transition occurred after the boundary layer exited the nozzle. Velocity traces were inspected 0.2 in. upstream; (this had to be done by intruding the probe into the flow on the other side of the nozzle, and thus it was checked only at the low value of $M_j = 0.31$). It was found that, for all cases, the characteristics of the velocity traces remained unchanged. Thus, the nominally laminar state originated from inside the nozzle.

Therefore, for $M_j > 0.35$, a nominally laminar state exists for the ASME design and long cases, while a turbulent state exists for the conic and the short-with-extension cases. At lower M_j the state may vary for some of the nozzles, however, the focus here is at high M_j where the noise measurements are performed. The state for the short case is also inferred to be turbulent although the reason for a high value of the shape factor has remained unclear. Note that as M_j is increased beyond $M_j > 0.6$ the ASME long case indicates a gradual drop in turbulence intensity and a gradual increase in momentum thickness. It is possible that its boundary layer tends to become turbulent as $M_j = 1$ is approached. The ASME short case exhibits opposite trends compared to the long case, as it will be seen with the noise data the Results section. Finally, an overall observation can be made based on the present and the earlier results in Reference 9. The differences between the nominally laminar and the turbulent cases seen with the present 2 in. nozzles are somewhat less pronounced compared to that found with the 1 in. nozzles in Reference 9. For example, in Reference 9, the transition to turbulence with the conic nozzle around $M_j = 0.3$ was much sharper, and the differences in turbulence intensity amplitudes between that and the design cases was somewhat larger. However, the differences in turbulance are still large enough to make consistent differences in the radiated noise, as discussed next.

Jet Noise Data

Preliminary Noise Data From the Flow Facility

Sound pressure level spectra measured in the CW17 facility for the different nozzles are shown in Figure 14. The data are for jet Mach numbers of 0.65 and 1.0, and shown as measured without any correction or nondimensionalization. The trip case data are presented separately in order to avoid clutter in Figure 14. The noise amplitude is conspicuously higher on the high frequency end for some of the nozzles. The trends become clearer with the same data shown only over the frequency range 20 to 40 kHz in Figures 14(c) and (d). The amplitudes for the ASME design case are the largest at both M_j. Amplitudes for the conic and the Sh-e cases are comparable and fall at the bottom of the band. Amplitudes for the ASME long and short cases are in between. Note that for the latter two nozzles, there is a switchover between the two Mach numbers. At $M_j = 0.65$ amplitudes for the long case are higher while at $M_j = 1.0$ they are lower, relative to the short case.

These trends are clearly captured by the partial OASPL values, integrated over 20 to 40 kHz range, shown as a function of M_j in Figure 15. Data are also shown for $\theta = 60°$ in addition to 90° and the trends are similar at either value of θ. The noise amplitude is clearly the highest with the ASME design case. It is low for the turbulent cases with the conic and the Sh-e nozzles. Amplitudes for the ASME short and long cases fall in between. For the latter two cases with increasing M_j there is the switchover in the amplitudes around $M_j = 0.85$. As noted with the boundary layer data, the trends suggest that with increasing M_j the boundary layer for the long case tends to become turbulent. As for the short case, we noted from velocity traces at $M_j = 0.32$ that the boundary layer is turbulent, but the noise data suggest that with increasing M_j it tends to become nominally laminar! The reason for this remains unclear; it is possible that compressibility effects play a role in this anomalous behavior.

The effect of boundary layer tripping with the ASME design case is shown in Figure 16 for the two values of M_j as in Figure 14. These data leave no doubt that the increased noise amplitude on the high frequency end occurs due to the highly disturbed laminar state of the boundary layer. When the boundary layer is turbulent, the amplitudes are the lowest.

Detailed Noise Data Taken in the Anechoic Facility

As stated before the noise measurements were later performed in the GRC AAPL, a high quality anechoic facility within NASA (Ref. 3). Because of busy facility schedules, only the ASME design, short-with-extension and the conic nozzles were tested. The data were acquired for cold flows covering a range of M_j. All spectral data were corrected for atmospheric attenuation and referenced to 1-ft distance from the nozzle. Figure 17(a) compares SPL spectra between the ASME design and the conic cases for $\theta = 90°$. A similar trend as seen in Figure 14 and in Reference 9 is confirmed. The noise amplitudes are clearly larger on the high frequency end for the ASME design case. The same data of Figure 17(a) are plotted in Figure 17(b) in 1/3rd-octave format. Overall, an unmistakable similarity with the spectral comparison in Figure 1 can be seen. With other possibilities ruled out in Reference 9 and with the high-quality data from the AAPL, one may infer that the anomaly discussed in the Introduction is most likely due to a difference in the initial boundary layer state. The exit boundary layers in References 4 to 7 were likely to be nominally laminar while those in References 1 to 3 were likely to be turbulent.

For the three nozzles investigated in the AAPL, all narrow band spectral data are provided in digital format. Here, some further comparisons are made. Figure 18 compares SPL spectra between the ASME design and the short-with-extension cases for four values of M_j. (When using the digital data one should note that there are some "dropouts" at low M_j; the bad data are marked with an amplitude value of 0.99. Also, there were some filtering issues at the high frequency end and 1-7992 data points were used ignoring the last 200 points.) The amplitude difference at high frequencies is seen to occur at all M_j.

Figure 19 shows that the amplitude difference also occurs at other polar locations and the difference is more pronounced at large values of θ. Directivity plots, OASPL versus θ, are shown in Figure 20(a). The noise amplitude is larger for the ASME design case over most of the θ-range; the difference is seen to vanish at the lowest end of the θ-range. Directivity for partial OASPL (amplitudes integrated over 20 to 40 kHz, as in Fig. 15) are shown in Figure 20(b). Once again, these data demonstrate the increased noise for the nominally laminar boundary layer case and, in general, a profound impact of the boundary layer state on the radiated noise.

Finally, flow visualization pictures are shown in Figures 21 and 22, in an effort to glean some insight into the flowfield differences that lead to the noise difference. In Figure 21, schlieren images are compared at three values of M_j between the ASME design and the short-with-extension cases; (for a description of the focused schlieren system the reader may look up Reference 14). It can be seen that the shear layers with the nominally laminar boundary layer state (ASME design) contains relatively more organized coherent structures. In comparison, the shear layers for the turbulent boundary layer state (Sh-e) are relatively more diffused. This is further illustrated with zoomed-in views in Figure 22 for another set of jet Mach numbers. Relatively more organized vortical structures can be seen to persist in the design case even at supersonic condition with shocks, at $M_j = 1.05$. The dynamics and interactions of the organized coherent structures are apparently responsible for the higher noise for the nozzles with the nominally laminar boundary layer.

Conclusions

Differences in subsonic jet noise databases from the literature were noted in previous work. Data taken in "University-type" facilities, involving higher contraction ratios and cleaner flows, were found to be of larger amplitudes relative to data taken in "Industrial-type" facilities. It had been inferred that a difference in initial boundary layer state might be the root cause for the anomaly. Further experimental study was conducted to confirm this inference. A set of 2-in. diameter nozzles was used to investigate the effect of varying exit boundary layer state on the radiated noise from high-subsonic jets. It was demonstrated that nozzles involving turbulent boundary layers are the quietest. Nozzles involving a nominally laminar state are characterized by significantly higher noise amplitudes especially on the high-frequency end of the spectrum. The latter boundary layer state involves a Blasius-like mean velocity profile but much higher turbulence intensity relative to that encountered in the turbulent boundary layer. The shear layers just downstream of the nozzle lip are characterized by more organized coherent structures. The dynamics and interaction of these coherent structures lead to higher turbulence as well as higher levels of high-frequency noise. All data as well as the nozzle coordinates are provided in digital format in an accompanying CD/DVD-ROM (available online from www.sti.nasa.gov) for anyone interested in further analysis.

References

1. Viswanathan, K., "Aeroacoustics of Hot Jets," *J. Fluid Mechanics*, 519, pp. 39–82, 2004.
2. Tanna, H.K., "An Experimental Study of Jet Noise Part I: Turbulent Mixing Noise," *J. of Sound and Vibration*, 50(3), pp. 405–428, 1977.
3. Lush, P.A., "Measurments of Subsonic Jet Noise and Comparison with Theory," *J. Fluid Mech*., 46(3), pp. 477–500, 1971.
4. Ahuja, K.K., "Correlation and prediction of jet noise," *J. of Sound & Vibration*, 29, pp. 155–168, 1973.
5. Olsen, W.A., Gutierrez, O. and Dorsch, R.G., "The Effect of Nozzle Inlet Shape, Lip Thickness, and Exit Shape and Size on Subsonic Jet Noise," *AIAA-73-187*, 11th AIAA Aerospace Sciences Meeting, Washington, Jan., 1973.

6. Harper-Bourne, M, "Commissioning and Validation of a New Jet Rig for the QinetiQ Noise Test Facility," *AIAA-2008-2958*, 14th AIAA/CEAS Aeroacoustics Conference, Vancouver, Canada, 5–7 May, 2008.
7. Bridges, J. and Brown, C.A., "Validation of the Small Hot Jet Acoustic Rig for Aeroacoustic Research," *AIAA-2005-2846*, 11th AIAA/CEAS Aeroacoustics Conference, Monterey, CA, 23–25 May, 2005.
8. Harper-Bourne, M., "Jet noise measurements: past and present," *Int. J. of Aeroacoustics*, 9(4&5), pp. 559–588, 2010.
9. Zaman, K.B.M.Q., "Effect of Initial Boundary Layer State on Subsonic Jet Noise," *AIAA J.*, 50(8), pp. 1784–1795, 2012.
10. Viswanathan, K. and Clark, L.T., "Effect of Nozzle Internal Contour on Jet Aeroacoustics," *Int. J. of Aeroacoustics*, 3 (2), pp. 103–135, 2004.
11. Schlichting, H., "Boundary Layer Theory," 7th Edition, McGraw Hill Book Company, New York, 1978.
12. Crighton, D.G., "Acoustics as a branch of fluid mechanics," *J. Fluid Mech*., 106, pp. 261–298, 1981.
13. Narasimha, R. and Srinivasan, K.R., 1979, "Relaminarization of fluid flows," *Advances in Applied Mechanics*, 19, pp. 221–309.
14. Zaman, K.B.M.Q., "Effect of initial condition on subsonic jet noise," *AIAA J., 23*(9), pp. 1370–1373, 1985.

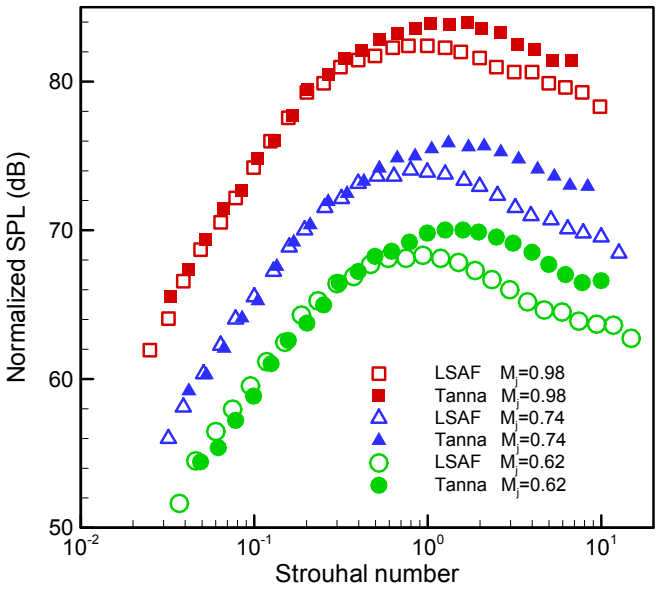

Figure 1.—Discrepancy in sound pressure level spectra (1/3rd-octave format) between measurements of Tanna and Viswanathan; $\theta = 90°$. Graph is copied from Reference 1.

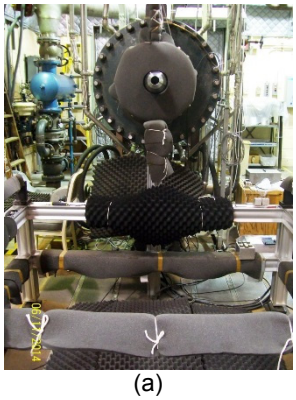

(a)

(b)

(c)

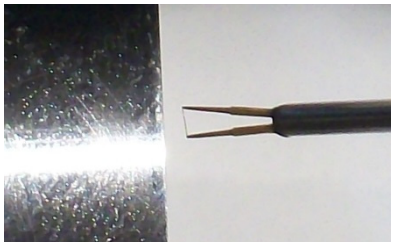

(d)

(e)

Figure 2.—Experimental Facility. (a) Open jet rig, (b) Conic nozzle, (c) ASME design nozzle, (d) hot-wire setup for exit boundary layer measurement, (e) rear view of ASME design nozzle with boundary layer trip, CAD drawing of the trip-sleeve on left.

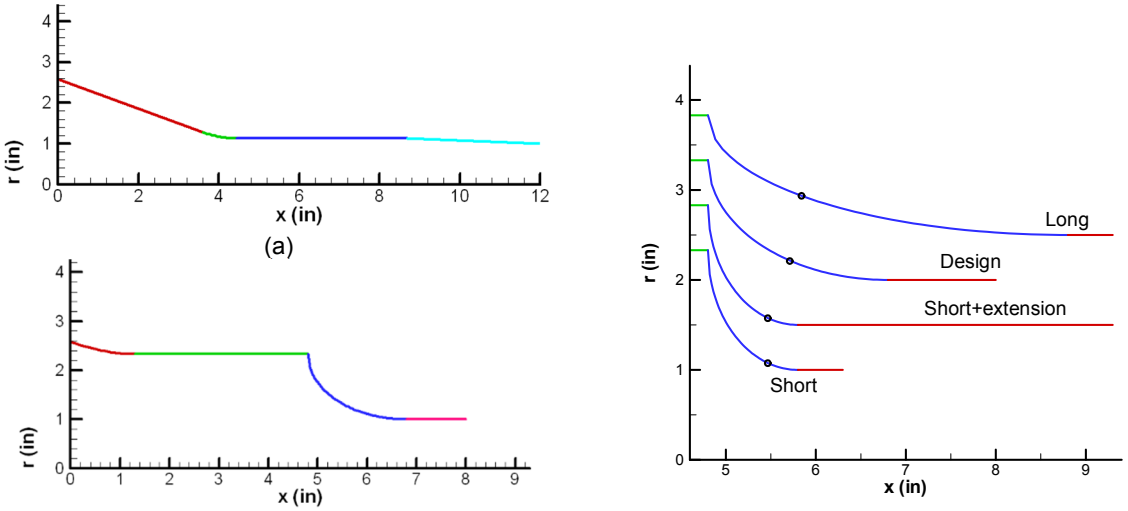

Figure 3.—Nozzle contours. (a) Conic, (b) ASME design, (c) convergent section of four ASME cases; ordinate pertains to the Short case and others are staggered by 0.5 in. black dots in (c) denote locations where "acceleration parameter" is equal to 2 (see text). (Four ASME cases, Fig. 3(c), are referred to as "Long", "Dsgn", "Sh-e", and "Shrt" in the following).

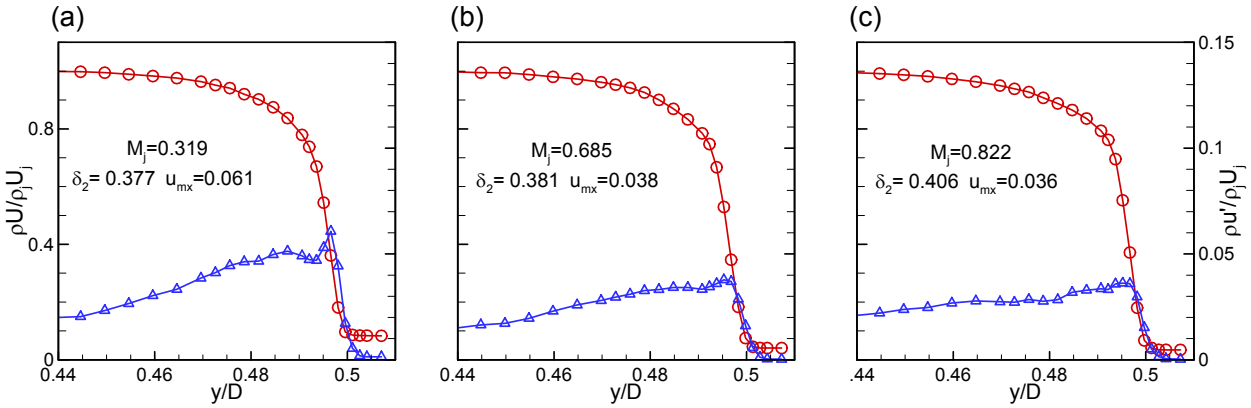

Figure 4.—Exit boundary layer data for conic case; circles (red) for mean velocity, triangles (blue) for turbulence intensity (scale on right). Momentum thickness (% of *D*) and peak turbulence intensity indicated in legend. Nominal jet Mach number, M_j: (a) 0.32, (b) 0.69 and (c).

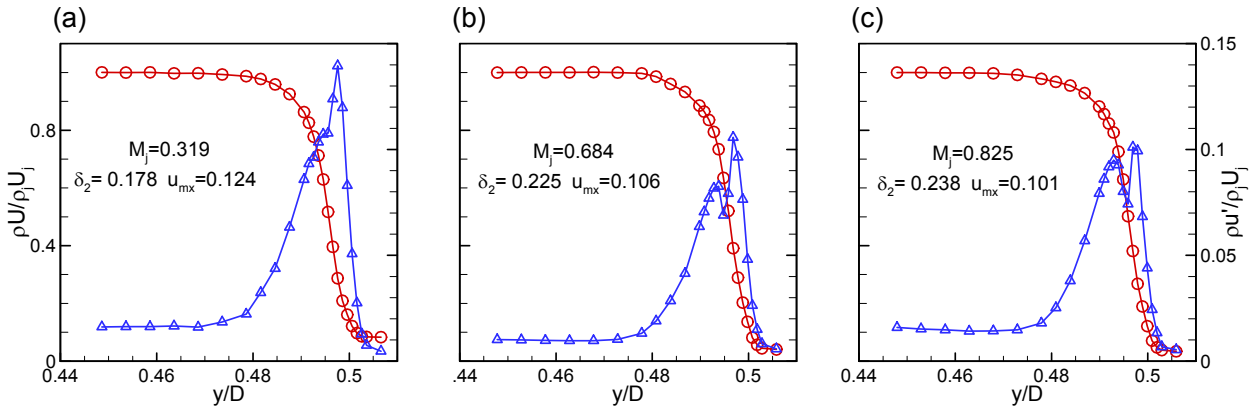

Figure 5.—Exit boundary layer data for Dsgn case, shown similarly as in Figure 4.

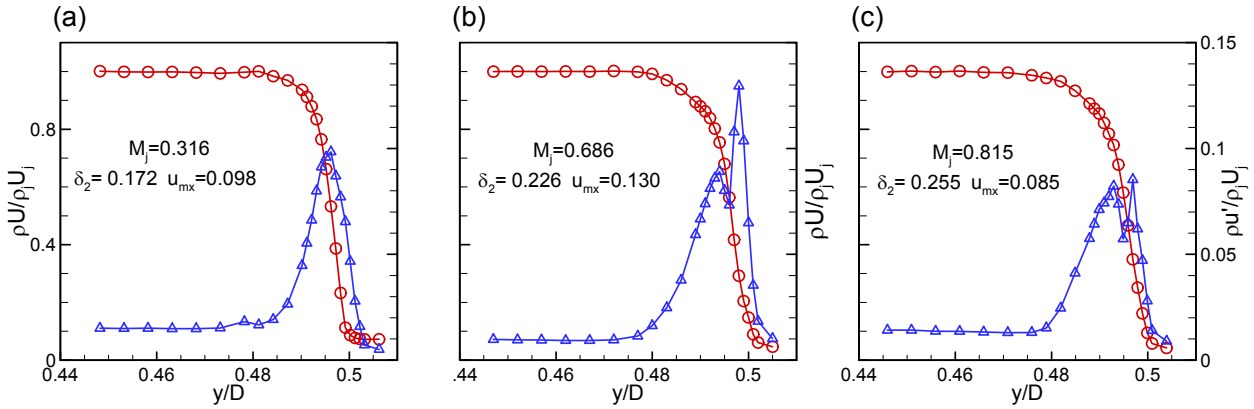

Figure 6.—Exit boundary layer data for Long case, shown similarly as in Figure 4.

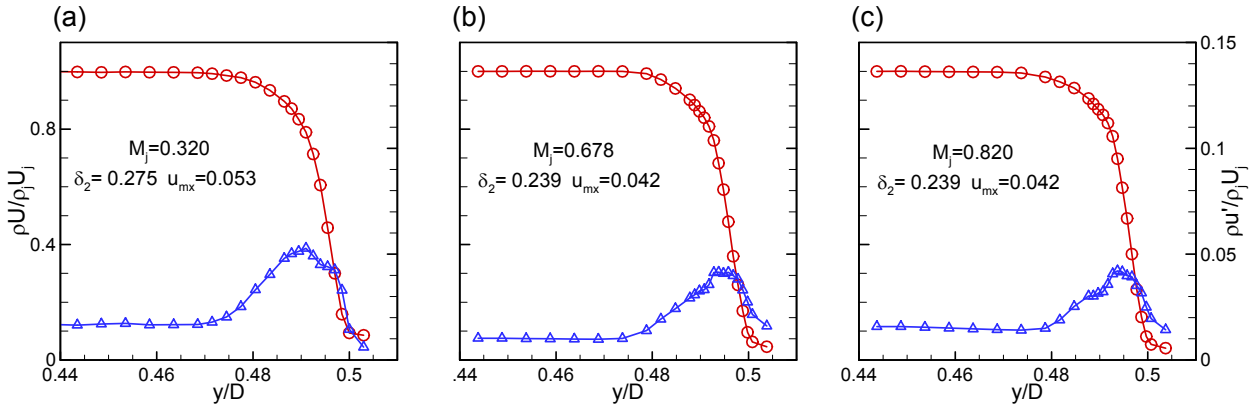

Figure 7.—Exit boundary layer data for Shrt case, shown similarly as in Figure 4.

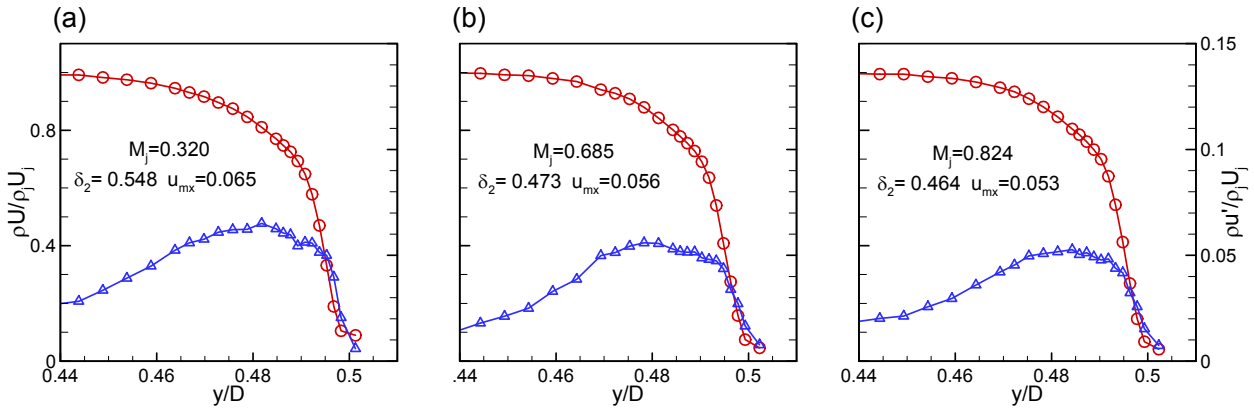

Figure 8.—Exit boundary layer data for Sh-e case, shown similarly as in Figure 4.

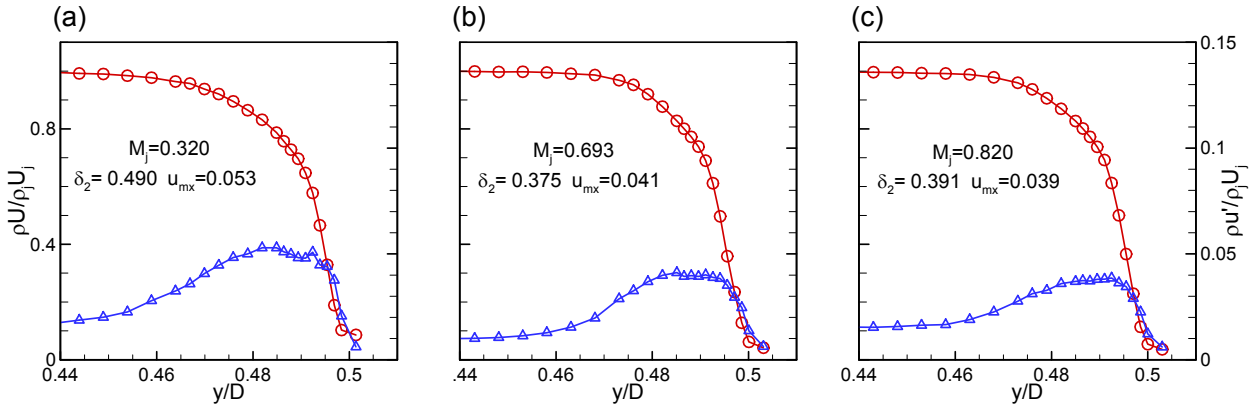

Figure 9.—Exit boundary layer data for the Dsgn case with boundary layer trip (Fig. 1(e)), shown similarly as in Figure 4.

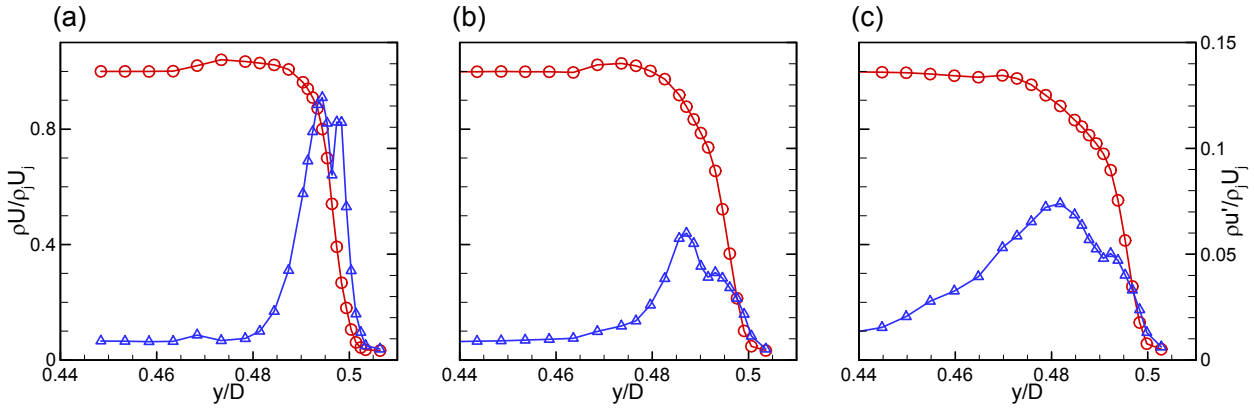

Figure 10.—Exit boundary layer data at M_j = 0.96 for three cases: (a) Dsgn, (b) Dsgn+trip, and (c) Sh-e.

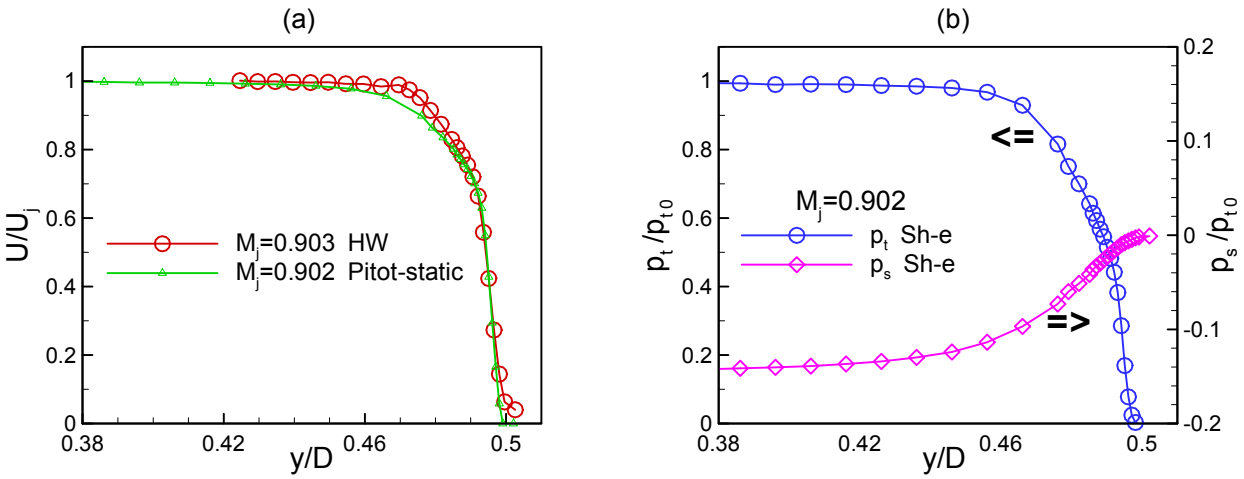

Figure 11.—Exit boundary layer profiles for the Short-with-extension case at M_j = 0.90. (a) Comparison of velocity profiles obtained by hot-wire and Pitot-static data. (b) Corresponding total and static pressure profiles.

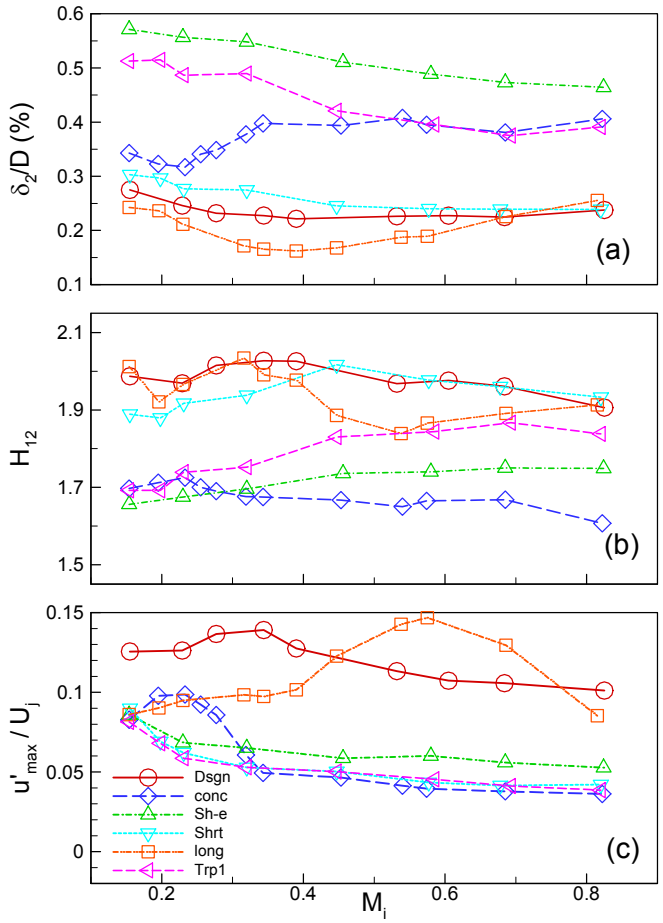

Figure 12.—Exit boundary layer characteristics versus M_j for the six nozzle cases. (a) Momentum thickness, (b) shape factor, and (c) peak turbulence intensity. Nozzle cases indicated in (c).

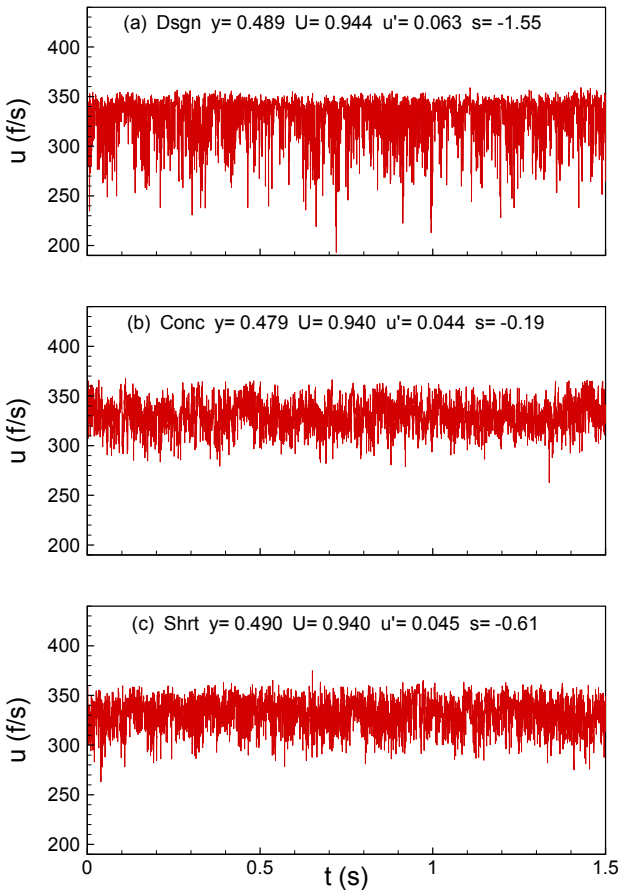

Figure 13.—Time traces of hot-wire signal at about 94 percent velocity point in the boundary layer for (a) Dsgn, (b) Conic, and (c) Shrt cases. Radial location (y/D), Mean velocity (U/U_j), turbulence intensity (u'/U_j) and skewness (s/u'^3) are indicated in legends; M_j = 0.31.

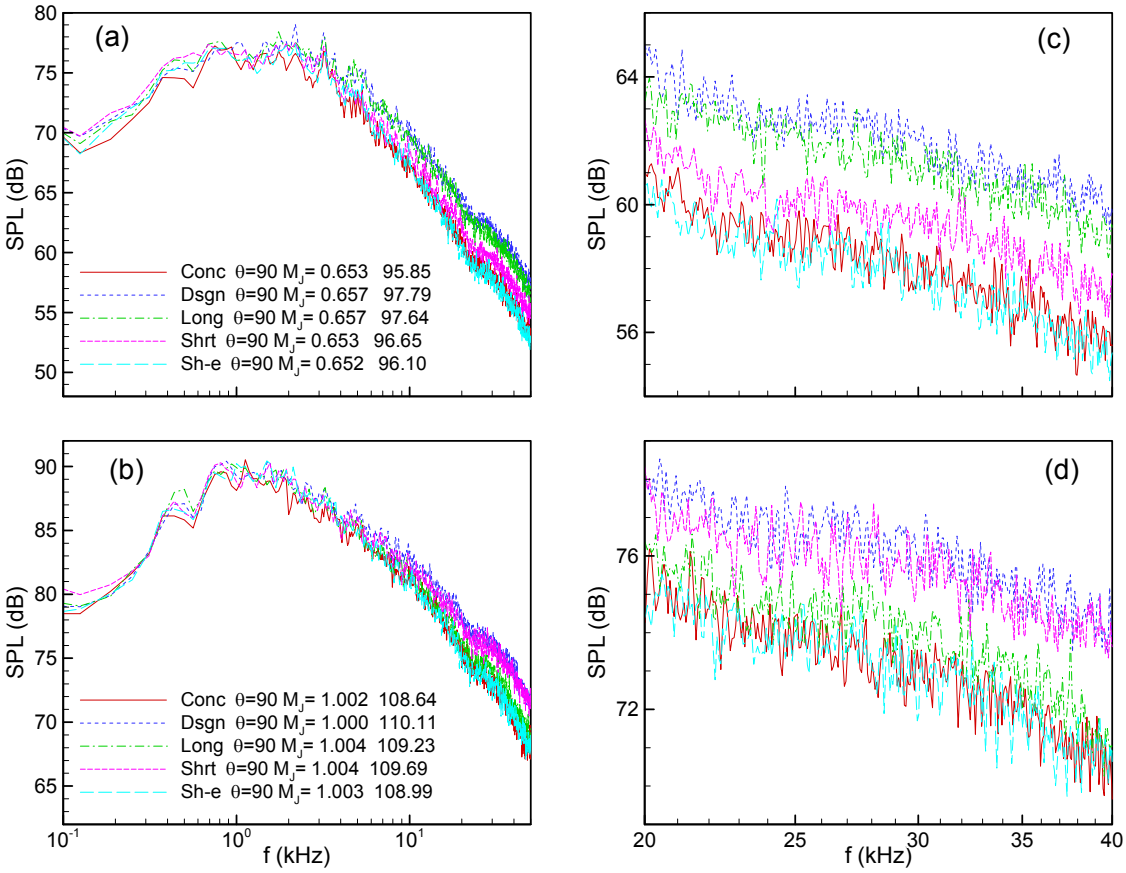

Figure 14.—Comparison of SPL spectra for five nozzles. (a) M_j = 0.66, (b) M_j = 1.00, (c) same data as in (a) shown over 20 to 40 kHz range, (d) same data as in (b) shown over 20 to 40 kHz range.

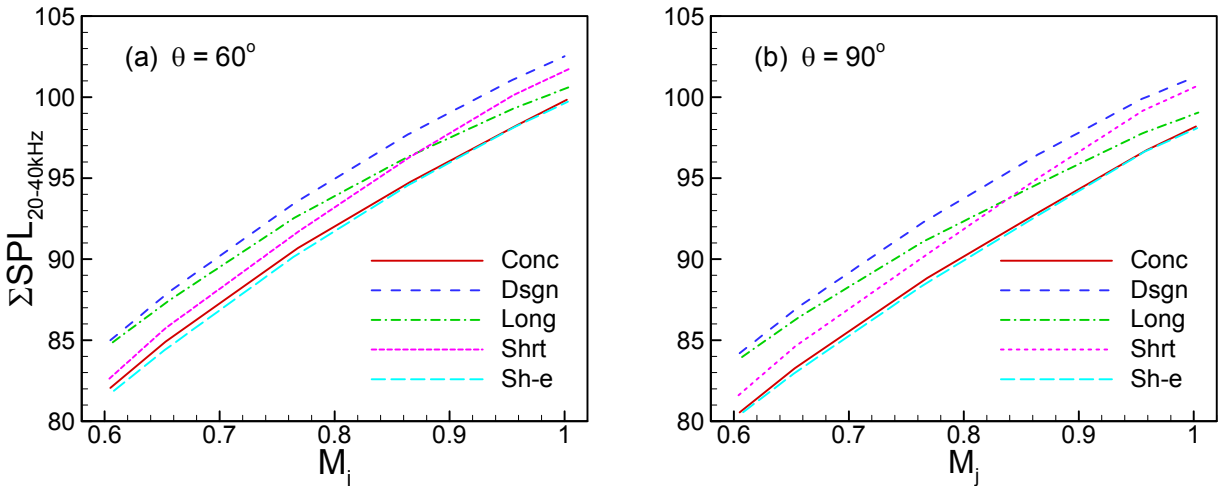

Figure 15.—Partial OASPL (integrated over 20 to 40 kHz range) for the five nozzles for two polar locations as indicated.

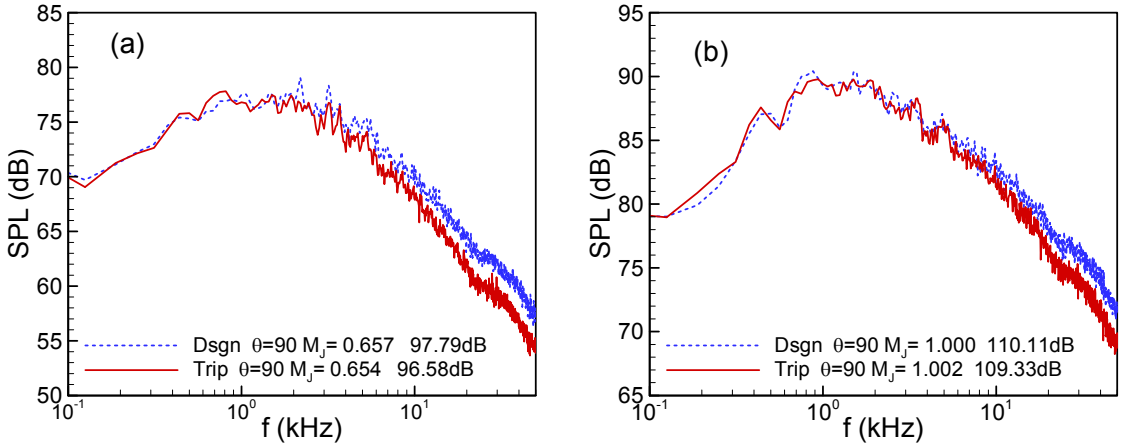

Figure 16.—SPL spectra for Dsgn case showing boundary layer trip effect: (a) M_j = 0.66, (b) M_j = 1.00.

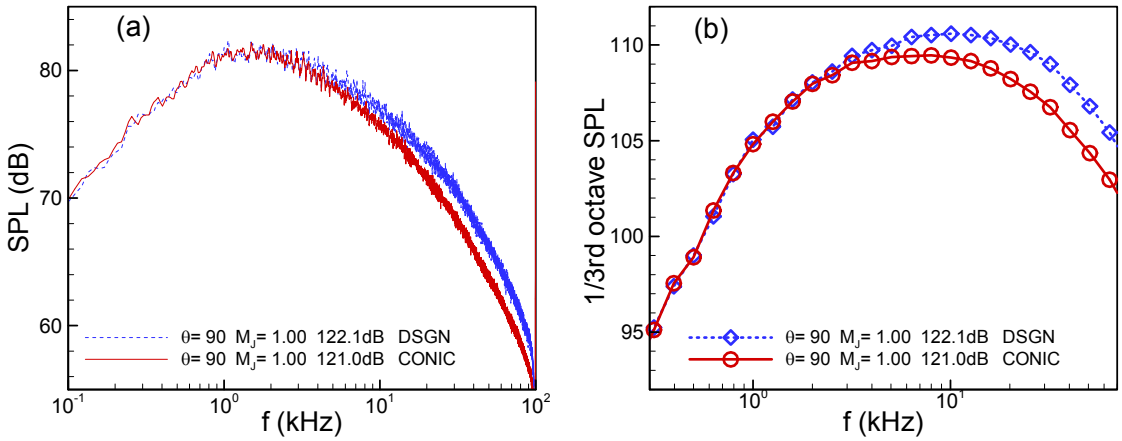

Figure 17.—Comparison of SPL spectra, obtained in the AAPL, between Conic and Dsgn cases. (a) PSD referenced to 1-ft distance, (b) same data in 1/3rd-octave format.

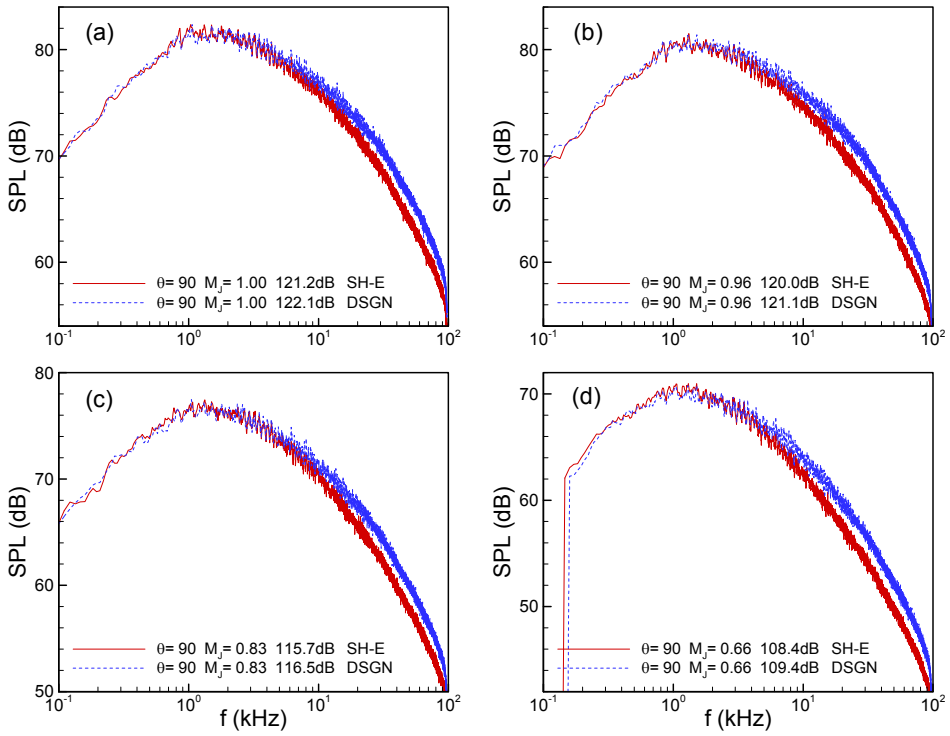

Figure 18.—Comparison of SPL spectra, obtained in the AAPL, between the Dsgn and Sh-e cases at θ = 90° for four jet Mach numbers: (a) M_j = 1.00, (b) M_j = 0.96, (c) M_j = 0.83, and (d) M_j = 0.66.

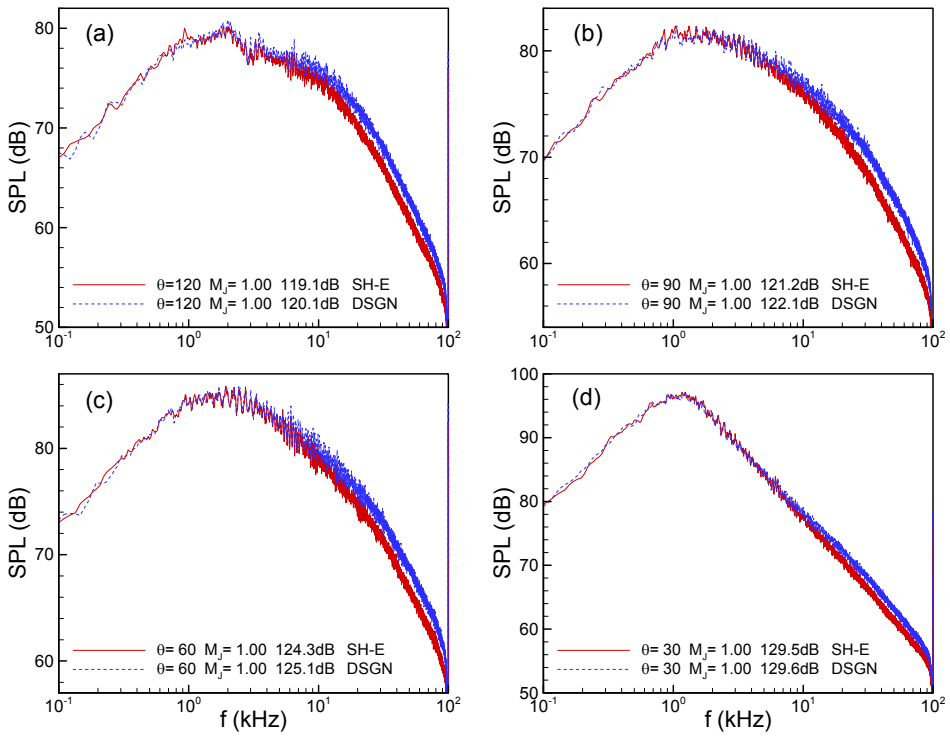

Figure 19.—Comparison of SPL spectra, obtained in the AAPL, between the Dsgn and Sh-e cases at M_j = 1.00 for four polar locations: (a) θ = 120°, (b) θ = 90°, (c) θ = 60°, and (d) θ = 30°.

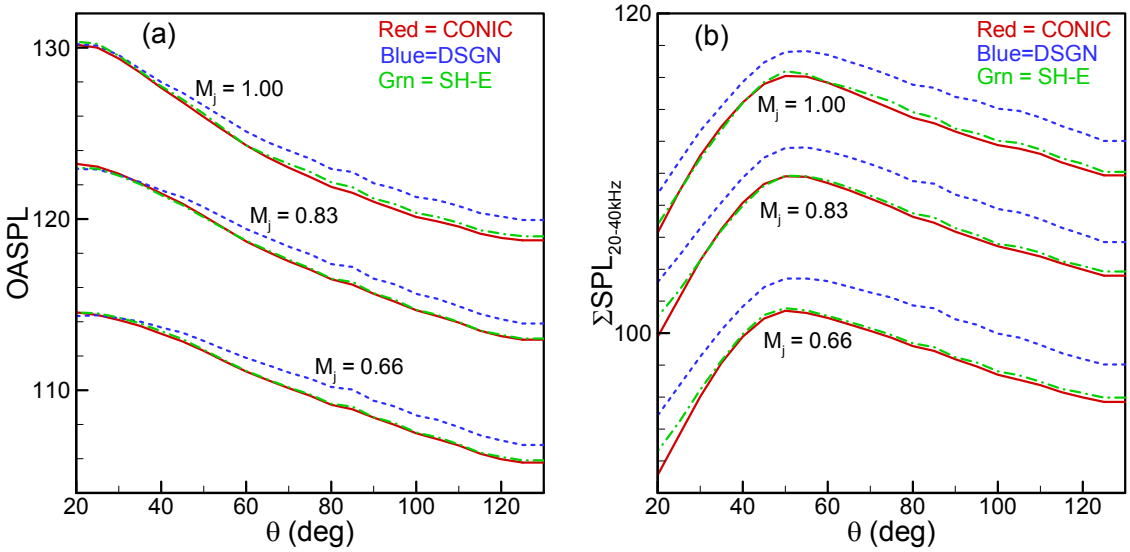

Figure 20.—Directivity plots from the AAPL data. Data for three nozzles as indicated at three values of M_j: (a) OASPL versus θ (b) Partial OASPL (integrated over 20 to 40 kHz range) versus θ.

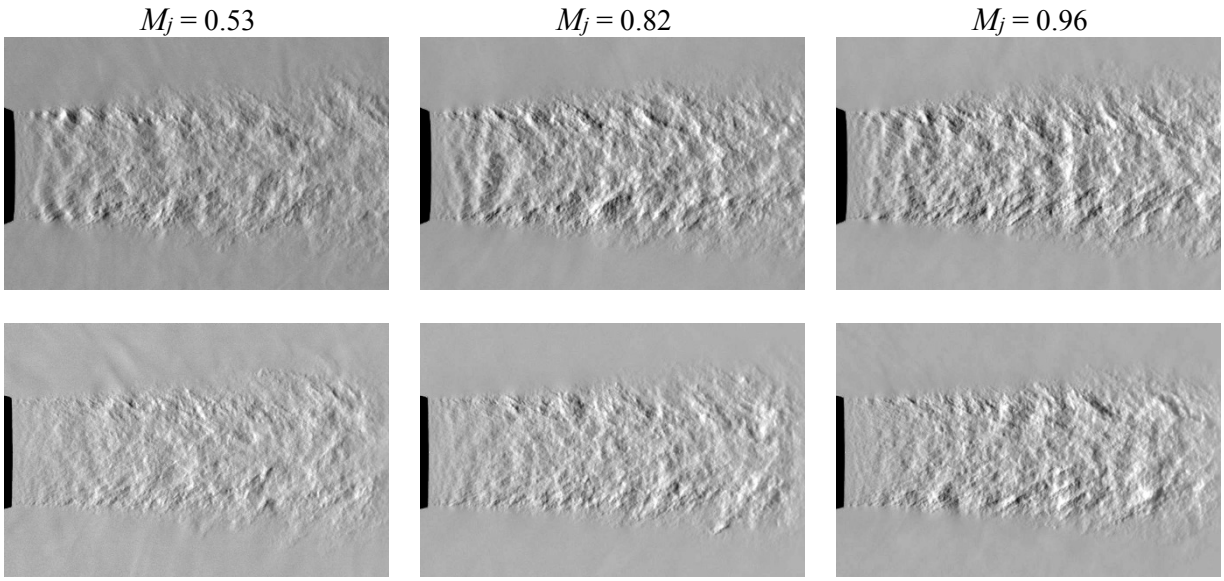

Figure 21.—Schlieren pictures of flowfield at three jet Mach numbers as indicated. Top row for Dsgn case, bottom row for Sh-e case.

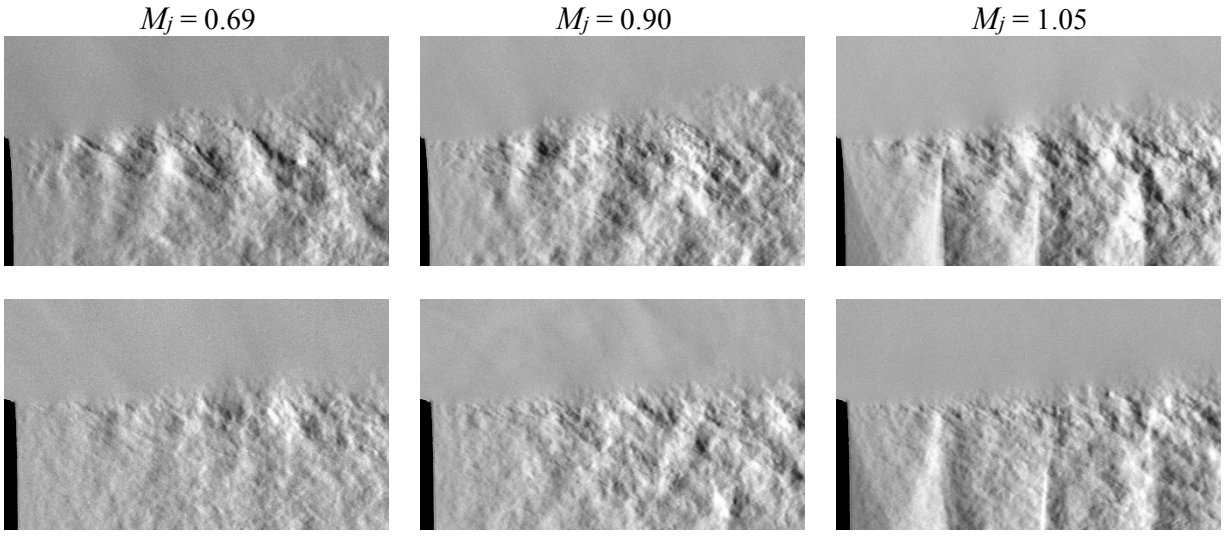

Figure 22.—Schlieren pictures of upper shear layer at three jet Mach numbers as indicated. Top row for Dsgn case, bottom row for Sh-e case.